Adsorption of phosphate and cadmium on iron (oxyhydr)oxides: A comparative study on ferrihydrite, goethite, and hematite

Jing Liu[1], Runliang Zhu[1]*, Lingya Ma[1], Haoyang Fu[1,2], Xiaoju Lin[1,2], Stephen C. Parker[3], Marco Molinari[3,4]

1. CAS Key Laboratory of Mineralogy and Metallogeny/Guangdong Provincial Key Laboratory of Mineral Physics and Materials, Guangzhou Institute of Geochemistry, Chinese Academy of Sciences (CAS), Guangzhou 510640, China
2. University of Chinese Academy of Sciences, Beijing 100049, China; Institutions of Earth Science, Chinese Academy of Sciences, Beijing 100029, China
3. Department of Chemistry, University of Bath, Claverton Down, Bath, BA2 7AY, UK
4. Department of Chemistry, University of Huddersfield, Queensgate, Huddersfield HD1 3DH, United King

* Corresponding author

Phone: 86-020-85297603

Fax: 86-020-85297603

E-mail: zhurl@gig.ac.cn

Abstract

Iron (oxyhydr)oxides participate in a variety of geochemical processes, and hence control the cycling of elements and quality of soils. The present work provides information about the macroscopic adsorption behaviors and microscopic mechanisms of typical cations and oxyanions (i.e., cadmium and phosphate) on three omnipresent iron (oxyhydr)oxides (i.e., ferrihydrite (Fh), goethite (Gt), and hematite (Hm)) in single- and double-solute systems, which can not only help in understanding the different adsorption behaviors of iron (oxyhydr)oxides, but also be important in developing robust and accurate surface complexation models. In both adsorption systems, Fh exhibited the strongest capacity in the uptake of phosphate and cadmium, followed by Gt and Hm; specifically, the adsorbed amounts of ions by Fh were ~6 times higher than those by Gt and Hm. Phosphate and cadmium can be synergistically adsorbed by the minerals. *In situ* attenuated total reflectance Fourier transform infrared (ATR-FTIR) spectra combining with the two-dimensional correlation spectroscopic (2D-COS) analysis were employed to unravel the bonding modes of phosphate on minerals. In the single-solute adsorption systems, although the primary species on Hm and Gt were similar, i.e., protonated and non-protonated bidentate phosphate complexes, more protonated complexes were found on Hm than on Gt; whereas the complexation modes of phosphate on Fh were diversified due to the complex nature of the surfaces, including monoprotonated bidentate, non-protonated bidentate, and outer-sphere complexes. The synergistic adsorption mechanisms of phosphate and cadmium on the three minerals were analogous, including electrostatic interaction, as well as the formation of phosphate-bridged ternary complexes and surface precipitation; nevertheless, the relative contributions of the mechanisms on the minerals were distinct: electrostatic attraction was the predominant co-adsorption mechanism for ions on Gt, while surface precipitation was the most significant on Fh among the three minerals.

This study can be enlightening to understand the interaction between the soil constituents, which is crucial to evaluate the fate and transport of the environmentally important substances in different geological settings.

Keywords: Cadmium; Phosphate; Ferrihydrite; Goethite; Hematite; Synergistic adsorption

1. Introduction

Iron (oxyhydr)oxides considerably contribute to the specific surface areas (SSA) of soils and possess a significant amount of reactive surface hydroxyl sites (Barrón and Torrent, 2013; Navrotsky et al., 2008), hence, they are regarded as important geosorbents and natural catalysts (Hiemstra, 2018; Lee et al., 2016; Pinney et al., 2009; Wade et al., 2018; Xu et al., 2019; Zhu et al., 2018). Among the various iron (oxyhydr)oxides, ferrihydrite (Fh) is the crystalline phase that initially forms after induced ferric hydrolysis in natural aqueous environments (Jambor and Dutrizac, 1998). The nanocrystalline Fh is ubiquitous in groundwater, stagnant water soils, and paddy soils (Barrón and Torrent, 2013). The metastable Fh can transform into Hm and Gt, which are very common constitutes in tropical soils such as ferralsols or oxisols (Barrón and Torrent, 2013; Yan et al., 2020). Generally, Fh converts to Gt through dissolution-recrystallization under acid or alkaline conditions, and to Hm under neutral pH through internal rearrangement (Barrón and Torrent, 2013; Cornell et al., 2003; Jiang et al., 2018). Hence, the distributions of iron (oxyhydr)oxides can be varied under different geological conditions. Since iron (oxyhydr)oxides have a high affinity to environmental substances (Arai, 2008; Elzinga and Sparks, 2007; Ona-Nguema et al., 2005; Silva-Yumi et al., 2018), the constitution of the chemicals in soils may exhibit spatial differences along with the distribution of different iron (oxyhydr)oxides.

The structures and surface properties of iron (oxyhydr)oxides exhibit similarities and differences, as revealed by previous studies (Barrón and Torrent, 2013; Cornell and Schwertmann, 2003a; Das et al., 2013; Hiemstra and Van Riemsdijk, 2009; Hinkle et al., 2015; Michel et al., 2007; Wang et al., 2013). All of the iron (oxyhydr)oxides consist of $Fe(O, OH)_6$ octahedron, and the surfaces of minerals expose abundant hydroxyl sites, including singly, doubly, and triply

coordinated hydroxyl groups. However, each iron (oxyhydr)oxide has varied arrangements of the $Fe(O, OH)_6$ octahedron. For instance, the needle-like Gt crystallites are made up of edge-sharing Fe octahedra chains cross-linked by double corners (Barrón and Torrent, 2013; Cornell and Schwertmann, 2003); Hm particles consist of hexagonal close packing of oxygens with cations distributing in the interstices of the octahedra (Barrón and Torrent, 2013, 1996; Cornell and Schwertmann, 2003); whereas the structures of Fh crystallites are similar to the Baker-Figgis δ-Keggin clusters and the particles are within the diameters of 2–10 nm (Barrón and Torrent, 2013; Michel et al., 2007). The structures and morphologies of the minerals dictate the surface properties of iron (oxyhydr)oxides. Plentiful studies suggest that the average densities of hydroxyl groups on Fh, Gt, and Hm are 2.0–7.9, 1.4–8.0, and 2.0–24.0 sites/nm^2 (i.e., 3.3–13.1, 2.3–13.28, and 3.3–39.8 μmol/m^2), respectively (Cornell and Schwertmann, 2003; Hinkle et al., 2015); the SSA values follow the sequence: Fh (200–600 m^2/g)>Gt (30–90 m^2/g)>Hm (10–90 m^2/g); and their pH values of point of zero charge (pH_{IEP}) range in 7.5–9.5 (Cornell and Schwertmann, 2003; Wang et al., 2013), indicating the surface of these minerals are positively charged under most environmental condition. As the structure and properties of iron (oxyhydr)oxides dictate their abilities in interacting with environmental chemicals, clarifying the exact surface reactivities of each iron (oxyhydr)oxides is critical for understanding their roles in affecting the character of soils.

The adsorption processes of ions on iron (oxyhydr)oxides determines the transport of the ions and the cycling of elements, which has been intensively studied (Ona-Nguema et al., 2005; Santoro et al., 2019; Singh et al., 2012; Swedlund et al., 2009; Trivedi and Axe, 2001; Wang and Xing, 2004; Wang et al., 2013; Zhang et al., 2019). Abundant evidence from laboratory studies suggests that the adsorption mechanisms of anions and cations on iron (oxyhydr)oxides may involve electrostatic attraction, ligand exchange, and surface precipitation (Catalano et al., 2008; Elzinga

and Kretzschmar, 2013; Ler and Stanforth, 2003). As the surface groups (e.g., Fe-OH) on iron (oxyhydr)oxides are quite similar, studies may quote the adsorption data and discuss the adsorption species and mechanisms on different iron (oxyhydr)oxides indiscriminately. However, a few previous studies also showed that the adsorption behaviors of ions on different iron (oxyhydr)oxides had certain distinctions (Arai, 2008; Ona-Nguema et al., 2005; Wang et al., 2013). For instance, As(III) formed a significant proportion of binuclear corner-sharing (^{2}C) complexes and a minor proportion of edge-sharing (^{2}E) complexes on Fh and Hm; in contrast, the As(III) on Gt formed dominantly binuclear corner-sharing (^{2}C) complex with a minor amount of monodentate mononuclear (^{1}V) complex (Ona-Nguema et al., 2005). These differences could be closely related to the atomic topologies, as well as physicochemical and electronic properties of the minerals surfaces: Gt possess a high proportion of double corner linkage (in favor of ^{2}C complexes formation), with few free edges (in favor of ^{2}E complexes formation), which only located at the terminal plane (001) (Cornell and Schwertmann, 2003); Hm possess abundant edges of the Fe(O, $OH)_6$ octahedra on the primary surfaces (e.g., (012) and (001)); whereas the surfaces of the nanosized Fh expose various types of reactive sites (Hiemstra and Van Riemsdijk, 2009). Thus, the ^{2}E complexes were found on the surfaces of Hm and Fh rather than on Gt. However, a systematic understanding of the similarity and distinction in adsorption behaviors of ions on different iron (oxyhydr)oxides is lacking.

The primary objective of the present study is to provide insights into the similarities and differences of the adsorption behaviors of ions (including oxyanions and heavy-metal cations) on varied iron (oxyhydr)oxides. Besides, as the chemical composition of the natural environment is complex, studying the adsorption of both single and multiple solutes on iron (oxyhydr)oxides could help to gain further understanding of the geochemical processes that operate in natural

systems (Brown and Sturchio, 2002). Although a few studies found that the adsorption of heavy metal cations and oxyanions on iron (oxyhydr)oxides could be inhibited by each other (Benjamin and Leckie, 1982), synergistic effects were observed in most of the co-adsorption studies (Li et al., 2007; Lin et al., 2017; Rietra et al., 2001; Simanova et al., 2011; Tiberg and Gustafsson, 2016; Villalobos et al., 2001; Wang and Xing, 2004). The synergistic adsorption of oxyanions and heavy-metal cations on iron (oxyhydr)oxides was attributed to electrostatic interaction and the formation of ternary complexes or surface precipitations. Generally, different mechanisms may contribute simultaneously to the co-adsorption of oxyanions and heavy-metal cations (Elzinga and Kretzschmar, 2013; Rietra et al., 2001; Simanova et al., 2011; Villalobos et al., 2001). Factors such as solution conditions, the nature and density of the adsorbate species, and the surface structure of the adsorbent may comprehensively influence the co-adsorption mechanisms (Collins et al., 1999; Li et al., 2007; Liu et al., 2018; Ostergren et al., 2000). However, understandings on how the surface properties and structures of iron (oxyhydr)oxides affect the synergistic adsorption behaviors and mechanisms of anions and cations are vague. In this study, Fh, Gt, and Hm were chosen as the representative iron (oxyhydr)oxides. The individual and simultaneous adsorption behaviors of cadmium and phosphate on Fh, Gt, and Hm were compared, and a particular focus was put on the ternary adsorption systems. The adsorption mechanisms were discussed based on *in situ* attenuated total reflectance Fourier transform infrared (ATR-FTIR) spectroscopy combining with two-dimensional correlation spectroscopic analysis (2D-COS).

2. Experimental section

2.1. Synthesis of iron (oxyhydr)oxides

$Cd(NO_3)_2 \cdot 4H_2O$, NaOH, HNO_3, $Fe(NO_3)_3 \cdot 9H_2O$, and NaH_2PO_4 of analytical grade (purity>99%) were obtained from Guangzhou Chemical Reagent Factory. 1 M of HCl and NaOH standard solutions were purchased from Shanghai Macklin Biochemical Co., Ltd. All of the reagents were used as received.

The three iron (oxyhydr)oxides were synthesized following the protocols described by Cornell and Schwertmann (2003). Fh was synthesized by adding a solution of $Fe(NO_3)_3$ (1 M, 100 mL) dropwise to a solution of NaOH (6 M, 50 mL) under vigorous magnetic stirring until the pH of the solution stabilized at 7. Gt was obtained by adding 180 mL of 5 M NaOH to a 100 mL solution of 1 M $Fe(NO_3)_3$. The suspension was immediately diluted to 2 L with twice distilled water and aged in a closed polyethylene flask for 60 h at 70°C. Hm was prepared by the forced hydrolysis of $Fe(NO_3) \cdot H_2O$ in a 0.002 M HNO_3 solution under 98°C for 7 d. The resulting suspensions were washed using ultra-pure water (0.055 μS/cm) and freeze-dried, and were allowed to pass a 200-mesh sieve before used as adsorbents.

2.2. Samples characterization

The X-ray diffraction (XRD) patterns of the minerals were recorded using a Bruker D8 ADVANCE X-ray diffractometer (Karlsruhe, Germany), operating at 40 kV and 40 mA using CuKα radiation. The SSA was measured using a Surface Area & Pore Size Analyzer from Quantachrome (Florida, USA). The samples were degassed at 80°C (Hm and Gt) for 12 h and 50°C (Fh) for 16 h under vacuum before the measurement. Scanning electron microscopy (SEM) (Carl

Zeiss SUPRA55SAPPHIR) and transmitted electron microscopy (TEM) (FEI Talos F200s) was used to detect the morphologies of the synthesized iron (oxyhydr)oxides.

Zeta potential measurements of Gt, Hm, Fh under various solution pH were carried out using a Malvern Zetasizer Nano-ZS (UK). Specifically, 0.05 g of the samples was added to 20 mL of 1 mmol/L $NaNO_3$ solution. The pH values of suspensions were then adjusted using 1M HNO_3 and NaOH solutions. The pH values were measured by pH-meter (PHS-3C, Shanghai LeiCi, China).

The surface sites of the samples were determined using the Gran plot method, which is commonly used to determine the total surface site densities of the minerals in contact with a solution (Liu et al., 2018). 0.2876, 0.4052, 0.8002 g of Fh, Gt, and Hm powders were individually added to 50 mL of 0.01 M NaCl solution and the Gran plots were calculated against a blank control (50 mL of 0.01 M NaCl solution). The suspensions were stirred on a magnetic stirring apparatus for 12 h. Afterwards, the solution pH was adjusted to 3 using the standard HCl solution (1 M) and then back-titrated to 11 using the standard NaOH solution (1 M). At last, the Grand plots were calculated based on the titration data.

2.3. Batch adsorption experiments

All of the batch adsorption experiments were carried out by adding 0.008, 0.05, and 0.08 g of Fh, Gt, and Hm, respectively, to 20 mL of 1 mM $NaNO_3$ solution containing different concentrations of cadmium and phosphate. Different amounts of minerals were added to obtain comparable data, as they show quite varied capacities in adsorbing target ions. The reactions occurred in 50 mL polypropylene bottles while they were vigorously shaken in an orbital shaker with a speed of 150 rpm at 25°C. Adsorption isotherms were measured using initial concentrations of 0.125–2 mM of cadmium and/or phosphate in the presence of minerals at initial solution pH 5.

Triplicate experiments were conducted with standard deviation presented in the figures. The values of $[Cd^{2+}]^3[PO_4^{3-}]^2$ under the experimental conditions were below the Ksp value of $Cd_3(PO_4)_2$ (2.53×10^{-33}) (Dean, 1999). $Cd(OH)_2$ is undersaturation in the experimental conditions as well. Hence, the precipitation of cadmium in the solution can be eliminated. In the ternary systems, to compare the distribution of cadmium and phosphate in solid and solution, the two kinds of ions were added with the same molar concentrations. The pH adsorption envelopes were measured with initial concentrations of 0.6 mM of cadmium and phosphate. The equilibrium solution pH values were measured, which are in the range of 3–6.5. Because it is hard to achieve exactly the same pH for triplicates, a series of samples at various pH values were used for each pH adsorption envelopes, rather than employing triplicates at fixed pH. After the reactions reached equilibrium (24 h), the polypropylene bottles were centrifuged at 6000 rpm for 10 min, and then the upper layer suspensions were passed through 0.22 μm filters for further analysis. The concentration of cadmium was determined by atomic absorption spectroscopy (Perkin Elmer AAnalyst 400, USA), and the concentration of phosphate was measured using the molybdenum method (Murphy and Riley, 1962) by UV-vis spectrophotometry (759S, Shanghai JingHua Instrument Co. Ltd., China).

2.4. *In situ* ATR-FTIR experiments

In situ ATR-FTIR measurements were conducted using a Bruker Vertex-70 FTIR spectrophotometer, equipped with a multi-bounce horizontal ATR accessory and flow cell (Pike Technologies). A horizontal ZnSe ATR crystal was coated with the film of minerals after 1 mL of 2 g/L iron (oxyhydr)oxides suspensions were air-dried on it. The solution pH was monitored throughout the experiment and adjusted by adding small amounts of 0.5 M HCl or 0.5 M NaOH. The mineral films were equilibrated with the background solution (1 mM NaCl), after which a

spectrum was collected as a background. The adsorption experiments were conducted with individual solutions of cadmium and phosphate circulated through a peristaltic pump at a rate of 1 mL/min. The initial concentrations of cadmium and phosphate were 50 μM, respectively. All of the spectra were collected at 25°C over a range of 400–4000 cm^{-1}, with a resolution of 4 cm^{-1} and 64 scans. At the end of each adsorption experiment, the mineral films were checked and no obvious erosion of the films was observed.

The FTIR spectra were analyzed based on the symmetry argument, which assigns molecular symmetry according to the number and position of bands. To better distinguish the overlapped bands, several spectra at equal time intervals were collected for the 2D-COS analysis proposed by Noda (Noda, 2014). The 2D contour plots were generated using the software "2D Shige" published by Shigeaki Mortia (Kwansei-Gakuin University, Japan). The numbers and positions of the vibration bands could be justified according to the 2D-COS analysis, the detailed description of the method is included in supporting information. Curve-fitting of the spectra was conducted using Gaussian line shape (Foerstendorf et al., 2014; Yang et al., 2016).

3. Results and discussion

3.1. Characterization of iron (oxyhydr)oxides

The powder XRD patterns show that the synthesized minerals were single-phase iron (oxyhydr)oxides (Fig. 1), according to the standard Joint Committee on Powder Diffraction Standards (JCPDS NO. 89-0598, 81-0598, and 29-0712). The two broad reflections at 2θ of 35° and 62° confirm that the synthesized Fh was 2-line Fh (Liu et al., 2016). The BET SSA of Fh, Gt, and Hm determined using N_2 adsorption-desorption isotherms (Fig. S1) followed the order: Fh

(316 m^2/g) > Gt (51 m^2/g) > Hm (36 m^2/g). It should be noted that the BET SSA of Fh is often below the "real" exposed surface area, because of the aggregation of Fh particles. According to the previously proposed empirical factor (Wang et al., 2013), the actual SSA can be ~464 m^2/g. The N_2 adsorption-desorption isotherms also indicate that Fh contains abundant micropore (0.14 cm^3/g, which is ~93% of the total pore volume), whereas Hm and Gt contain little micropore (<0.01 cm^3/g). The SSA values and microporosities of the minerals were in the range of the previously proposed values (Cornell and Schwertmann, 2003; Wang et al., 2013). The differed SSA values and pore structures should be linked to the micro-morphologies of the three minerals. The morphologies of the three minerals were determined using SEM and TEM (Fig. 1). Fh consisted of numerous aggregated fine nanoparticles; the needle-like Gt was 100–800 nm in length and 10–30 nm in width; whereas Hm was in spindle form with a particle size of ~40 nm.

The pH_{IEP} of the samples increased in the order Fh (8.4)<Gt (9.3)<Hm (9.6), as unraveled by the zeta potential measurements (Fig. 2A); According to the Gran plots (Fig. 2B), the surface sites densities of Fh, Gt, and Hm were 2.12, 7.98, 3.75 sites/nm^2 (i.e., 3.52, 13.25, 6.23 μmol/m^2), respectively. Among the three minerals, Fh has the most negatively charged surfaces, the highest SSA value, and the lowest site density. The data of these properties are in accord with those proposed in the previous studies (Hiemstra et al., 2009; Hinkle et al., 2015; Liu et al., 2018). These differences in structure and surface properties might cause varied adsorption behaviors of ions on the three minerals. For instance, the differences in surface area and densities of surface sites of the three minerals should lead to varied adsorbed amounts of ions, besides, the varied surface charges shall affect the partition of anions and cations on Fh, Gt, and Hm.

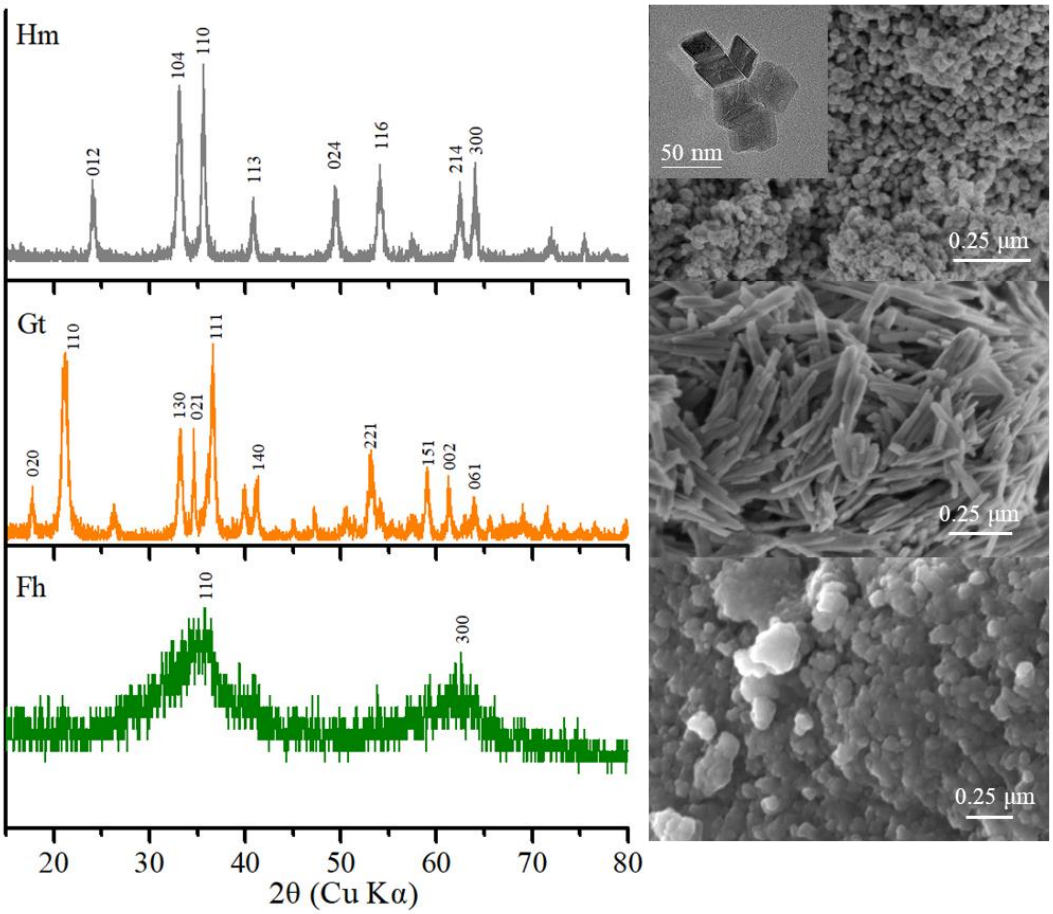

243

244 Fig. 1.XRD pattern, SEM, TEM images of the synthesized ferrihydrite (Fh), goethite (Gt),

245 and hematite (Hm)

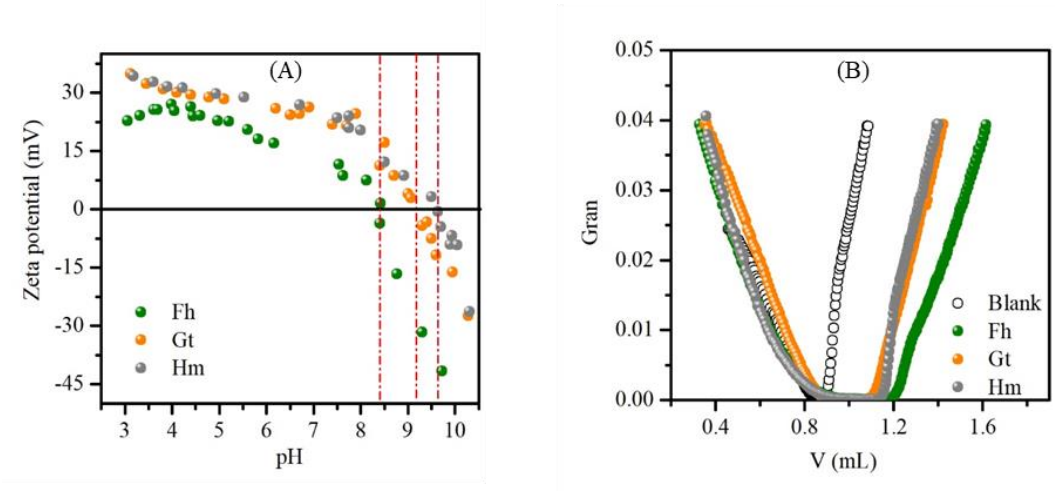

246

247 Fig. 2.Surface zeta potentials (A) and Gran plots (B) of the three minerals (2.5 g/L mineral

suspension were used for zeta potential test; Fh, Gt, and Hm powders were individually added to 0.01 M NaCl solution for the acid-base titration)

3.2. Adsorption of phosphate and cadmium on iron (oxyhydr)oxides

3.2.1. Adsorption isotherms

As shown in the adsorption isotherms of phosphate and cadmium on Fh, Gt, and Hm in the binary adsorption systems (Fig. S2A and B), Fh displayed the strongest adsorption capacities toward phosphate and cadmium, followed by Gt and Hm. The adsorption of phosphate on Fh reached a plateau at the equilibrium concentration of ~0.55 mM, after which the adsorbed amounts mildly increased to 0.6 mM. The adsorption capacities of phosphate on the minerals in the adsorption isotherms decreased in the order Fh (0.6 mmol/g)>Gt (0.1 mmol/g)>Hm (0.05 mmol/g). The adsorbed amounts of phosphate on the minerals were very close to the results under similar solution conditions proposed in the previous studies (pH 4.5): Fh (0.8–1.0 mmol/g)>Gt (~0.1 mmol/g)>Hm (~0.06 mmol/g) (Wang et al., 2015, 2013). The isotherm data were analyzed using Langmuir and Freundlich isotherm models (Fig. S2A). The adsorption isotherms were fitted better with Freundlich equations, and the constants and R^2 values for different systems are given in Table S2. The high values of n indicate high affinities of the three minerals to phosphate. Besides, the n values indicate a rank of affinities of the minerals to phosphate, which is consistent with the rank of the adsorption capacities. The adsorption of cadmium followed the same sequence. Nevertheless, the affinities of minerals toward cadmium were much weaker than those toward phosphate (Fig. 2A). Due to the extremely weak adsorption of cadmium on the minerals (removal ratios were ~10% at different points), the adsorption isotherms were hard to be fitted using the isotherm models. The weak adsorption characteristic of cadmium is in accordance with the previous studies. Specifically,

the adsorbed amounts are in the range of the previously proposed adsorbed amounts of cadmium the minerals (e.g., 0.2–0.4 mmol/g on Fh and <0.1 mmol/g on Gt and Hm) under comparable conditions.

When phosphate and cadmium were co-existed in the solutions (at a molar ratio of 1:1), they were synergistically adsorbed on the three minerals (Fig. 3A and B). At the low equilibrium concentration (≤0.2 mM), the adsorbed amounts of phosphate were roughly the same as those in the absence of cadmium, possibly due to the low concentration of cadmium and the high affinity of phosphate to the surface (i.e., rather limited effect of cadmium on enhancing the adsorption of phosphate). At higher equilibrium concentrations (≥0.2 mM), the adsorbed amounts of phosphate were enhanced enormously by cadmium, which increased by 2.9, 1.3, and 3.6 times on Fh, Gt, and Hm at the final points of the adsorption isotherms. It is noteworthy that the adsorption isotherm of phosphate in the Fh system shows a sharp increase after a plateau. As discussed by previous studies (Farley et al., 1985), the formation of a new phase (surface precipitation of cadmium and phosphate) could be a reasonable explanation for the sharp increase of the slope in the adsorption isotherms. However, such a phenomenon was not presented in the Gt and Hm systems, which could be ascribed to the significantly lower loading of ions on these minerals.

The adsorption isotherms of cadmium in the presence of phosphate reveal that the adsorbed amounts of cadmium were evidently enhanced by phosphate, even at low initial concentrations (<0.4 mM) (Fig. 3B). With the increase of solute concentrations, the removal efficiencies of cadmium first increased and then decreased mildly, the removal efficiencies are ~40% on Fh, and ~20% on Gt and Hm, floating within an amplitude of 11% (Table S1). At the initial concentrations beyond 0.8 mM, the adsorption of cadmium increased slower with the increasing concentration of ions in Gt and Hm adsorption systems, whereas the removal rates of cadmium kept invariable in

293 the Fh system. The amounts of cadmium adsorbed on the three minerals are less than those of
294 phosphate, and the difference between the adsorbed amounts of phosphate and cadmium became
295 less significant with the increasing loading of ions. The synergistic behavior of phosphate and
296 cadmium should be related to electrostatic interaction and the potential formation of ternary
297 complexes or even surface precipitation, as indicated in previous studies (Elzinga and Kretzschmar,
298 2013; Hinkle et al., 2015; Tiberg and Gustafsson, 2016). The synergistic adsorption mechanisms
299 will be discussed in detail in later sections.

300 The batch adsorption experiments indicate that both in the binary and ternary adsorption
301 systems, Fh has the best capacity in the uptake of these two ions. These results are coincident with
302 those in the previous studies (Cornell and Schwertmann, 2003; Wang et al., 2013), which proposed
303 that Fh with extremely high surface area should exhibit stronger adsorption capacities to ions as
304 compared to the other iron (oxyhydr)oxides. In the binary systems, the removal amounts of
305 cadmium by Gt and Hm are similar, but the adsorption of phosphate on Gt is superior to that on
306 Hm. In the ternary systems, the adsorbed amounts of phosphate are similar on Gt and Hm, while
307 the adsorbed amount of cadmium on Gt is higher, indicating different distribution ratios of the two
308 ions on the iron (oxyhydr)oxides. The ratios of the adsorbed amounts of phosphate and cadmium
309 on the three minerals will be compared and discussed below.

310 **3.2.2. pH adsorption envelopes**

311 The pH conditions in natural aquifers have a significant influence on the adsorption of ions
312 on iron (oxyhydr)oxides. Rising pH could influence the ions adsorption by generating more
313 anionic forms or less cationic form of the ions (e.g., $H_2PO_4^-$ and HPO_4^{2-} for phosphate and
314 $Cd(OH)^+$ for cadmium), as well as causing the decrease of surface $FeOH_2^+$ and increase of FeO^-

groups (Hiemstra and van Riemsdijk, 2009). Previous studies provide abundant information about the effects of solution pH on the adsorption of phosphate and cadmium in binary systems. Rising pH would decrease the adsorption of anions, while increase the immobilization of cations (Antelo et al., 2015). In particular, phosphate exhibits a strong affinity to iron (oxyhydr)oxides. The adsorption of phosphate on iron (oxyhydr)oxides is significant over a wide pH range (3–9), with the adsorbed amounts being reversely related to the solution pH (Antelo et al., 2015; Carabante et al., 2010). For the adsorption of cadmium, the plots of adsorbed amount versus pH are mostly sigmoidal, and the adsorption capacity could increase from 0 % to 100% in a specific pH range (Tiberg and Gustafsson, 2016). The pH values where the removal percentage of cadmium reach 50% in the pH envelopes were~5.5–7 for Gt and Fh and ~7–8.5 for Hm, which are dependent on the concentration of cadmium and the minerals (Jiang et al., 2013; Komárek et al., 2018; Pivovarov, 2001; Ponthieu et al., 2006; Rout et al., 2012; Swedlund et al., 2009; Wang and Xing, 2004).

In the ternary systems in this study, the change of the adsorbed amount of phosphate under different pH is unobvious, the variations of the data are within 6% (Fig. 4A and Table S3). On the contrary, the adsorption of cadmium increased evidently with the increase of solution pH (Fig. 4B and Table S3). As shown in Table S3, with the solution pH increases from 3.4 to ~5.78, the removal percentages of cadmium increased from 0.13 to 0.49 on Fh, 0.11 to 0.43 on Gt, and 0.098 to 0.41 on Hm. When the solution pH changed in the same amplitude, the removal percentages of increased 2.8, 2.9, and 3.2 times on Fh, Gt, and Hm, respectively. The shape of the pH envelopes of cadmium in this study is different to those in the work of Tiberg and Gustafsson (2016), which should be caused by the much higher dosage of Fh and concentration of cadmium in our study. It should be noted that the saturation index calculations using 0.6 mM phosphate and 0.6 mM cadmium show that the solution at pH $\geq$ 5.78 is oversaturated with respect to $Cd_3(PO_4)_2$. Hence,

when the adsorption of phosphate and cadmium on iron (oxyhydr)oxides is not considered, the homogeneous precipitation of $Cd_3(PO_4)_2$ shall happen at pH ≥ 5.78. In the ternary adsorption system, the homogeneous precipitation of $Cd_3(PO_4)_2$ in the presence of the three minerals cannot happen even at pH 6.5 from the perspective of thermodynamics (Table S4). Even if homogeneous precipitation happens at beginning of the adsorption reaction, it would dissolve with the proceeding of the reaction due to the decrease of the concentration of solutes in solution. Heterogeneous precipitation may contribute to the co-adsorption processes at the experimental conditions, as the oversaturation of heterogeneous precipitation can achieve at a lower concentration than homogeneous precipitation (Ler and Stanforth, 2003).

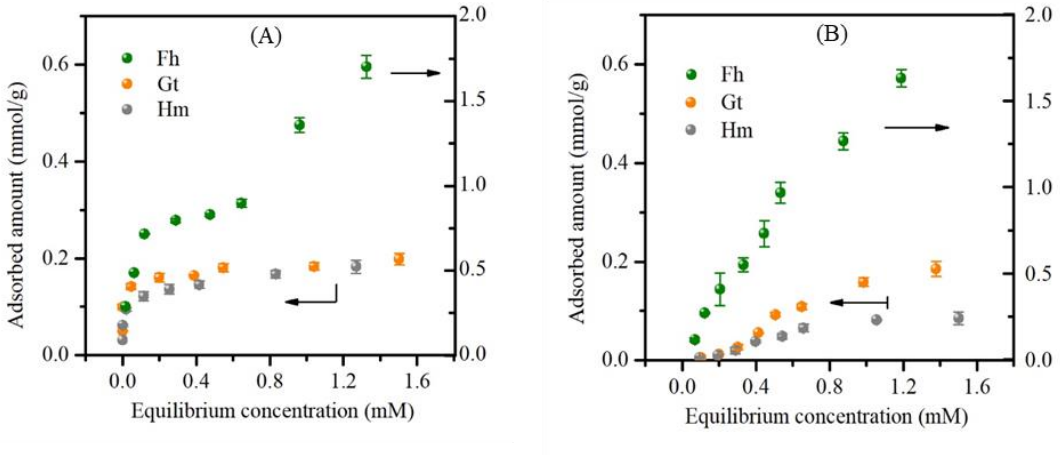

Fig. 3.Adsorption isotherms of phosphate (A) and Cd(II) (B) in the ternary systems on Fh, Gt, and Hm (the adsorbed amounts of ions on Gt and Hm were on the left ordinate, and those on Fh were on the right ordinate; the initial concentrations of phosphate were equal to those of Cd(II))

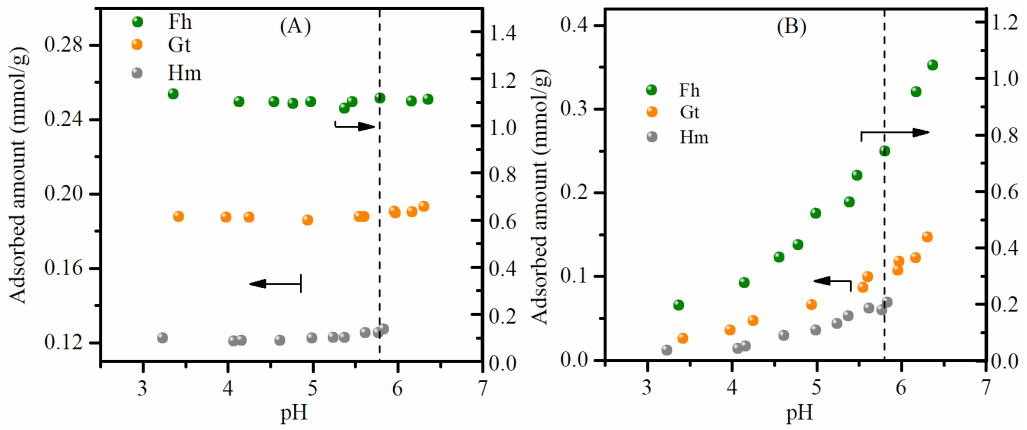

Fig. 4.pH adsorption envelopes of phosphate (A) and Cd(II) (B) on Fh, Gt, and Hm in the ternary systems. The dashed lines refer to the pH values where the precipitation of Cd3(PO4)2 start to happen if the adsorption is not taken into considerations (the pH values of suspensions after the equilibrium of adsorption reactions were measured and used as the x-coordinates. The adsorbed amounts of ions on Gt and Hm were on the left ordinate, and those on Fh were on the right ordinate)

3.2.3 Distribution ratios of cadmium and phosphate on iron (oxyhydr)oxides

The distributions of anions and cations on iron (oxyhydr)oxides when they were co-adsorbed could not only affect the transport of the corresponding ions, but also control the growth of secondary minerals on iron (oxyhydr)oxides. For instance, the growth of oxysalt minerals (e.g., (Ce, La)[PO_4], $Ni_3(H_2O)_8[AsO_4]_2$) can be affected by iron (oxyhydr)oxides (Milton et al., 1944; Wang et al., 2018). For better extracting information from the data, the ratios of the adsorbed phosphate/cadmium (PO_4/Cd) versus the surface coverage (Fig. 5A) were plotted based on the data in adsorption isotherms. At low surface coverage (calculated according to the specific surface area and the adsorbed amounts of cadmium and phosphate), the ratios of PO_4/Cd reached ~8.9, 5.1, and 2.7 on Gt, Hm, and Fh (Fig. 5A), respectively, suggesting extremely higher affinity of the minerals toward phosphate over cadmium. With the increase of surface coverage, the ratios of PO_4/Cd

gradually dropped toward 1, indicating that anions and cations could be equally immobilized on the minerals at high surface coverage, where the adsorption mechanisms might be distinct to those at low surface coverage. Besides, the ratios of PO_4/Cd on the three minerals at the same surface coverage were distinct, and they increased by the sequence of Fh<Gt<Hm at the surface coverages ranging from 0.001 to 0.002 mmol/m^2, which is in the same sequence of the surface potentials of the three minerals. The ratios of PO_4/Cd as a function of equilibrium solution pH are presented in Fig. 5B. At equilibrium solution pH ~3.3, the adsorbed amounts of phosphate are ~10.0, 7.2, and 5.8 times higher than those of cadmium. The ratios of PO_4/Cd on the three minerals at the same pH follows the same sequence of the surface potentials of the minerals, as well. The ratios decreased sharply when the solution pH increase from ~3 to 5, and the difference between the minerals diminishes when solution pH values are above 5. The ratios approach to 1 at pH ~6.4 for Gt and Fh. The positive correlation between the PO_4/Cd ratios and the surface potentials of minerals indicates that the surface electrical properties of the minerals should play important roles in determining the partition of anions and cations on the minerals (Hiemstra and Van Riemsdijk, 2009; Ler and Stanforth, 2003).

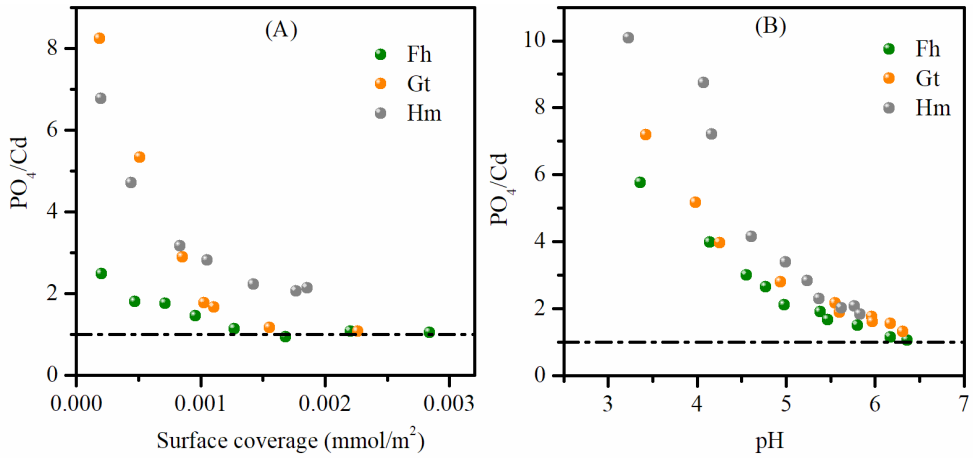

Fig. 5.Relationships of the adsorbed amounts ratios of phosphate and Cd(II) (i.e., PO4/Cd) with the surface coverage (A) and the equilibrium solution pH (B) of the minerals

3.3 Adsorptive characteristics of ions on different iron (oxyhydr)oxides

3.3.1 Comparison of the adsorption mechanisms of phosphate on iron (oxyhydr)oxides

To get in-depth information on the interactions between ions and iron (oxyhydr)oxides in the binary and ternary adsorption systems, in situ ATR-FTIR spectra of phosphate on Fh, Gt, and Hm were collected under the environmentally related pH condition (5 and 7). The 2D-COS analysis was employed to better distinguish the overlapped bands. As indicated in previous studies (Elzinga and Sparks, 2007; Kubicki et al., 2012), multiple phosphate complexes may form on iron (oxyhydr)oxides simultaneously, and figuring out all of the adsorbed phosphate complexes is impractical. Hence, only the dominant complexes that could be recognized in 2D-COS analysis will be considered in this study. Taking the 2D spectra of the complexes on Gt at pH 5 in binary systems as examples (Fig. 6A and B), the synchronous spectra display the synchronous correlation between three bands: 1100, 1044, and 947 cm^{-1}, suggesting the species with these three bands should be the dominant complex on Gt. This species has been previously recognized as non-protonated bidentate complex (Arai and Sparks, 2001). The asynchronous spectra indicate another set of bands at ~1125, 1055, and 1000 cm^{-1}. Previous studies suggest that the band at 1120 cm^{-1} representing ν(P=O) and the band at 1008 cm^{-1} representing ν_{as}(P-$(OFe)_2$ belong to the monoprotonated bidentate complex (Elzinga and Sparks, 2007). However, that species include vibration bands at 1117, 1007, and 960 cm^{-1}, among which the former two bands are consistent with those in this study. As the band at 1055 cm^{-1} is very close to that at 1044 cm^{-1}, the signal was considered to be the result of the distortion. Besides, the spectra of phosphate complex on Gt showed intense noise at frequencies below 960 cm^{-1}, possibly due to the vibration of the mineral and the bands below 960 cm^{-1} will not be discussed in the Gt systems. Hence, phosphate could be

primarily adsorbed as (1) the protonated bidentate complex with the vibration bands at 1125 and 1000 cm^{-1}, and (2) the non-protonated bidentate complex with the vibration bands at 1100 and 1044 cm^{-1} on Gt. The synchronous and asynchronous spectra of phosphate on Gt at pH 7 revealed bands similar to those at pH 5.

The deconvolution of the spectra (Fig. 6C) was conducted according to the 2D analysis results. The bands belonging to the same spectra grow or decreased consistently in certain proportions, which further support our previous assignment to the bands. With the increase of solution pH, the bands of non-protonated complex increased while the bands of the protonated complex decreased proportionally. The bonding modes of phosphate on Gt in this study are consistent with those proposed by Luengo et al (2006). Besides, the spectra of 2D-COS are similar to the results reported by Yang et al. (2016) who proposed the co-presence of mono-protonated and non-protonate bidentate complexes on Gt at pH 6. However, the di-protonated bidentate complex formed at pH 3 proposed by Yang et al. was not found in this study, possibly due to the differences of solution pH (the solution pH values in this study were in the range of 5–7).

The synchronous and asynchronous spectra in Hm and Fh adsorption systems and the detailed analysis of the spectra are summarized in the supporting information (Fig. S4–5). The asynchronous signals in the spectra suggest that at least two types of phosphate complexes could form on Hm and Fh in the binary systems. The spectra in Fig. 6D and E were deconvoluted according to the corresponding 2D-COS analysis results. The non-protonated bidentate complex with bands (green-tinted) located at ~1080, 1048, and 950 cm^{-1} was detected on Hm and Fh, similar to those on Gt. The bands' positions of the same kind of complex show slight differences in the three minerals, which could be ascribed to the varied effects of different surfaces on electronic structures of the adsorbed phosphate complexes (Elzinga and Sparks, 2007). The second

complexes on Hm with vibration bands (gray-tinted) at ~1120, 1000, and 934 cm^{-1} were similar to those formed on Gt, which should be protonated bidentate complex as illustrated above.

The spectra of phosphate complexes on Fh were much overlapped. In addition to non-protonated complexes, the other complexes formed on Fh were different from those on Gt and Hm. At pH 5, the species with bands at 1110, 1028, and 992 cm^{-1} could be protonated monodentate complex (Arai and Sparks, 2001); whereas at pH 7, the complexes with vibration bands at 1100 and 970 cm^{-1} could be outer-sphere surface complex, as these bands are similar to those of HPO_4^{2-} (aq) (Liu et al., 2018). Similar broad FTIR bands of phosphate on Fh were observed by Arai and Sparks (2001), who assigned the complexes formed at pH $\geqslant$ 7.5 as non-protonated bridging phosphate complexes, and the species forming at pH 4 as protonated bridging complexes. The difference in our results with those in the study of Arai and Sparks could be attributed to the following reasons: the ferrihydrite that synthesized in different conditions may differ largely in the microstructure even when they were in the same mineral phase as checked by XRD, and hence may result in varied adsorption characteristic of ions on Fh (Michel et al., 2007); besides, the varied reaction conditions in different works also have influences on the adsorption mechanisms. These differences further suggest that experiments conducted at resembled conditions are needed to make clear comparisons of the adsorption reactions on the surfaces of different minerals.

To sum up, the adsorption mechanisms of phosphate on Gt, Hm, and Fh show similarities and distinctions, which were heavily dependent on the solution pH. The non-protonated bidentate complex was the predominant complex on all of the three minerals at pH 7. Similarly, Kim et al. (2011) proposed that the phosphate ions bond via two oxygen ions (i.e., bidentate complex) to all of the investigated iron (oxyhydr)oxides surfaces (i.e., goethite, akageneite, and lepidocrocite) using ^{31}P static spin-echo mapping NMR experiments. Such similarities in the adsorption

mechanisms of phosphate may exhibit on most iron (oxyhydr)oxides on which hydroxyl groups act as the functional sites. The favorable formation of the bidentate complex over monodentate complex on iron (oxyhydr)oxides is mainly related to the fact that the former complex is energetically favored (Ona-Nguema et al., 2005). With the decrease of solution pH (pH 5), the proportion of non-protonated bidentate complex decreased, and the adsorbed complexes on the three minerals became varied. On one hand, the adsorbed species on Fh were different from those on Gt and Hm, which is possibly due to the diversity of surface sites on Fh deriving from the amorphous nature and extremely small diameter. On the other hand, the protonation state of the phosphate complexes on the three minerals differed significantly. While the complexes formed on Fh were not protonated at pH 7, the protonated complexes do exist on Gt and Hm, and the protonation states of species on Hm were more significant than those on Gt. As demonstrated in previous studies, the adsorbed anions were more easily protonated than those in bulk water, due to the differences in the entropy of solvent molecules (Tejedor-tejedor and Anderson, 1990).

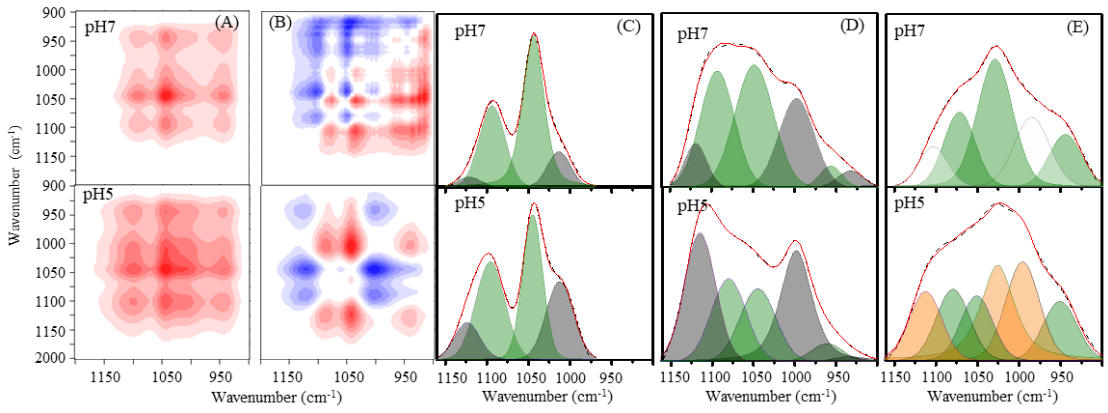

Fig. 6.Synchronous (A) and asynchronous (B) contour plots obtained from the 2D-COS analysis of the infrared spectra of phosphate complexes on Gt at pH 5 and 7 in the binary systems; the FTIR spectra of the adsorbed phosphate on Gt (C), Hm (D), and Fh (E) in the binary systems. (The peaks with the same color refer to the phosphate complexes in the same molecular symmetry)

3.3.2 Comparison of the co-adsorption mechanisms of phosphate and cadmium on iron (oxyhydr)oxides

In the ternary systems, the 2D plots of phosphate spectra on Fh were distinct to those in the binary systems. However, in the Gt and Hm reaction systems, the 2D plots of phosphate spectra in the binary and ternary adsorption systems were similar. To compare the surface complexes in the binary and ternary adsorption systems, difference spectra (the spectra in ternary systems minus those in the binary systems) were calculated and resolved according to the major complexes distinguished in the 2D-COS analysis.

In the Gt reaction systems, the shapes of the difference spectra (Fig. 7A) were similar to those in binary systems (Fig. 6C), indicating the types and proportions of the primary phosphate complexes were similar in the presence and absence of cadmium. Hence, the non-protonated bidentate complex should be the dominant species on Gt in the ternary systems. It should be noted that the bands at ~1125 cm^{-1} in the difference spectra were particularly higher and became more significant with the decrease of solution pH, while the other bands kept changing in specific proportions. Specifically, the ratios of the peak area at 1044 cm^{-1} to those at 1100 cm^{-1} are 1.05 and 1.70 for the phosphate spectra on Gt at pH 5 and 7, and 1.57 and 1.31 for the corresponding difference spectra; whereas the ratios of the peak area at 1125 cm^{-1} to those at 1000 cm^{-1} are 0.44, 0.29, 1.32, and 0.96 for the above spectra. As compared to those in the binary system, ratios between the peak at 1125 cm^{-1} to 1000 cm^{-1} are more than 3 times higher in the difference spectra, which changes much significant than the ratios between the peaks at 1044 cm^{-1} to 1100 cm^{-1}. A reasonable explanation could be that the peak at 1125 cm^{-1} belongs to another kind of complex. Hence, in addition to non-protonated and protonated bidentate complexes, a new complex with P=O vibration shall form on Gt. On the surfaces of Hm, the resolved difference spectra (Fig. 7B)

suggest that non-protonated bidentate complex was the dominant increasing species with the addition of cadmium. Nevertheless, the proportion of the P=O vibration band decreased with the decrease of solution pH, which was on the contrary to those in the Gt system. The difference spectra of phosphate in Fh reaction systems were similar to those on Hm under neutral condition. When only the two major species were considered, the proportions of the non-protonated bidentate complex in the resolved difference spectra (Fig. 7C) on Fh were slightly smaller than those on Hm. As the pH of solution declined, the proportion of the species with P=O vibration in the difference spectra increased, which was consistent with the scenarios on Gt, while contrary to those on Hm.

The co-adsorption mechanisms of oxyanions and cations could be influenced by the solution pH, adsorption density, the affinities of adsorbates to surfaces, and the properties of minerals surface, as proposed in previous studies (Elzinga and Kretzschmar, 2013; Hinkle et al., 2015; Liu et al., 2016). The formation of surface precipitation and ternary complexes, as well as electronic interaction, are considered to be the primary reasons for the co-adsorption of heavy-metal cations

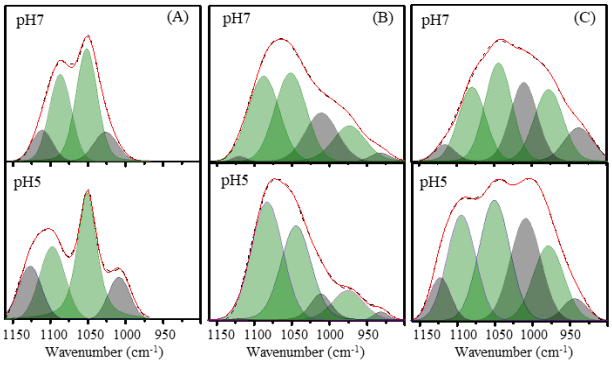

Fig. 7.The difference spectra between the spectra of phosphate complexes in the ternary systems and binary systems on Gt (A), Hm (B), Fh (C). J. Liu et al.

and oxyanions on iron (oxyhydr)oxide (Ler and Stanforth, 2003; Li and Stanforth, 2000; Nooney et al., 1998; Tiberg and Gustafsson, 2016). For instance, Ler and Stanforth (2003) suggested the formation of surface precipitation on Gt during the adsorption process of phosphate based on the

change of surface zeta potential. Nooney et al. (1998) provided direct evidence of phosphate precipitation on Hm using an atomic force microscope, in which large terraces and islands with a diameter of hundreds of nanometers were observed on the Hm surfaces. Although both of the two studies investigated the adsorption of phosphate in the absence of cations, reactions in these studies include the dissolution of Fe(III) from minerals and the multi-layer adsorption of phosphate and Fe(III) on the surfaces of minerals. In ternary adsorption systems, the CD-MUSIC model calculation by Rietra et al. (2001) suggested that the synergistic adsorption of phosphate and Ca(II) was attributed to the electrostatic interactions between the ions with opposite charges. Tiberg et al. (2013 and 2016) proposed that the co-adsorption of phosphate with Cd(II), Cu(II), Pb(II) should include the formation of metal-bridged ternary complexes as supported by the results of EXAFS and the three-plane CD-MUSIC simulation. On the contrary, Antelo et al. (2015) believed that the synergistic adsorption of Ca(II) with phosphate and arsenate was attributed to the formation of the anion-bridged complex using the CD model. The varied co-adsorption mechanisms proposed in different studies could be attributed to the distinctions in reaction conditions, and clear recognition on the similarities and differences of the co-adsorption mechanisms on Gt, Hm, and Fh can hardly be obtained based on results from various studies.

Under comparable conditions, the co-adsorption behaviors of phosphate and cadmium on Gt, Hm, and Fh were investigated individually in this study. The adsorption isotherm of phosphate on Fh indicates the formation of surface precipitation at high ions concentration (>0.6 mM). Surface precipitation of phosphate and cadmium on Gt and Hm couldn't be fully excluded based on the shape of the isotherms, as the transition from adsorption to precipitation is not always obvious in the adsorption isotherms when precipitation begins to happen. Nevertheless, the adsorption isotherms of phosphate suggest that the surface precipitation of phosphate and cadmium on Fh

should be more significant than those on Gt and Hm (even if the precipitations have formed).

The ATR-FTIR analysis further reveals the similarities and distinctions in the adsorption mechanisms of ions on the three minerals in the ternary systems. The difference spectra (spectra in ternary systems minus those in the binary systems) in the three minerals reaction systems include a significant proportion of non-protonated bidentate complexes, which were in similar positions with the same species in the binary systems. The increase of non-protonated bidentate phosphate complexes in the presence of cadmium suggests that cadmium may enhance the interaction between phosphate and the iron (oxyhydr)oxides, possibly through modifying the surface charge of the mineral surfaces. As the non-protonated complexes were the dominant increasing species with the addition of cadmium on Gt (Fig. 7A), electrostatic interaction should play a dominant role in the co-adsorption of ions on Gt under the experimental conditions. From the above analysis, electrostatic interaction should be one of the major causes of the synergistic adsorption of phosphate and cadmium on the three minerals. This finding is in accordance with Tiberg and Gutafsson (2016) who propose that electrostatic interactions should contribute to the synergistic adsorption of phosphate and cadmium on ferrihydrite. Nevertheless, their EXAFS and SCM results reveal that the increased adsorption of cadmium by phosphate cannot be explained by electrostatic interactions alone, which has also found in this study.

The incongruous increase of P=O peak in the difference spectra in Gt reactions systems suggests that the peak should be involved in another kind of complex, which could increase with decreasing pH, in addition to the protonated bridging complex. On the surfaces of Hm, the non-protonated bridging complex was the dominant increasing species under the experiment conditions, and the relative proportion of the species with P=O vibration decreased remarkably with the decreasing pH. The complex with P=O vibration on Gt and Hm, which changed in a contrary way,

could either be protonated bridging complex or phosphate acting as a bridge of cadmium and the surface (phosphate-bridged ternary complexes). The most reasonable interpretation is that the presence of cadmium promoted the formation of the latter complexes, similar to the explanation in the study of Antelo et al. (2015) and Tiberg and Gutafsson (2016). The P=O vibration on the minerals should be attributed to the formation of both complexes. The contrary change of the P=O vibrations with solution pH on Gt and Hm could be attributed to the favorable formation of the protonated bridging complex on Hm, since the transformation from protonated bridging complexes to phosphate-bridged ternary complexes does not contribute to the increase of P=O vibration. On account of the possibility of such transformation, the dominance of electrostatic attraction and ternary complexes formation cannot be clearly determined on Hm. On the surfaces of Fh, the complex structure of the surfaces made the spectra of adsorbed phosphate to be highly overlapped, but the newly emerged complex with P=O vibration can be a clue of the formation of phosphate-bridged ternary complexes.

4. Conclusions and implications

The distributions and constitutions of iron (oxyhydr)oxides are distinct in different geological settings. Therefore, a comparison of the reactivities of various iron (oxyhydr)oxides has important geochemical and environmental implications. This study systematically unravels the similarities and differences in the adsorption behaviors and mechanisms of phosphate and cadmium on three omnipresent iron (oxyhydr)oxides (i.e., Fh, Gt, and Hm), combining with the physicochemical properties of the minerals. All of the three minerals favored accumulating phosphate over Cd, and they could adsorb the two ions synergistically in ternary systems. Although phosphate ions were

predominantly adsorbed as non-protonated bidentate complexes on the three minerals in the binary systems, Hm favored the formation of protonated bidentate complexes as compared to Gt, while the species on Fh were diversified due to the complex nature of the surfaces. On the other hand, the synergistic adsorption mechanisms of phosphate and cadmium in the ternary systems were investigated. Although the ternary systems are rather complex, they are important analogies to the complicated nature systems. To unravel the molecular-level problems posed by the complex natural systems, multidisciplinary/interdisciplinary approaches are needed. Results in this study suggest that the synergistic adsorption mechanisms of phosphate and cadmium on the three minerals are similar, including electrostatic interaction and the formation of phosphate-bridged ternary complexes or surface precipitation; however, the contributions of different mechanisms are varied on the three minerals: the formation of surface precipitation should be more significant on Fh than those on Hm and Gt, and the synergistic adsorption of phosphate and cadmium on Gt was primarily attributed to electrostatic attraction. Such differences in the co-adsorption mechanism shall affect the long-term immobilization of the ions in different soils with different constitution of the iron (oxyhydr)oxides. Furthermore, the ratios of the adsorbed amounts of anions and cations are varied significantly on the three minerals, indicating that the formation of secondary phases on these iron (oxyhydr)oxides, which could happen in nature, may also be distinct.

Acknowledgments

This work was supported by the National Key Research and Development Plan of China (2016YFD0800704), National Natural Science Foundation of China (41872044), China

602 Postdoctoral Science Foundation (2019M663132), and the Newton Advanced Fellowship
603 (NA150190).

604

References

1. Antelo, J., Arce, F., Fiol, S., 2015. Arsenate and phosphate adsorption on ferrihydrite nanoparticles. Synergetic interaction with calcium ions. Chem. Geol. 410, 53–62.
2. Arai, Y., 2008. Spectroscopic evidence for Ni(II) surface speciation at the iron oxyhydroxides-water interface. Environ. Sci. Technol. 42, 1151–1156.
3. Arai, Y., Sparks, D.L., 2001. ATR–FTIR spectroscopic investigation on phosphate adsorption mechanisms at the ferrihydrite–water interface. J. Colloid Interface Sci. 241, 317–326.
4. Barrón, V., Torrent, J., 2013. Iron, manganese and aluminium oxides and oxyhydroxides. Eur. Mineral. Union Notes Mineral. 14, 297–336.
5. Barrón, V., Torrent, J., 1996. Surface Hydroxyl configuration of various crystal faces of hematite and goethite. J. Colloid Interface Sci. 177, 407–410.
6. Benjamin, M.M., Leckie, J.O., 1982. Effects of complexation by Cl, SO_4, and S_2O_3 on adsorption behavior of Cd on oxide surfaces. Environ. Sci. Technol. 16, 162–170.
7. Brown, G.E., Sturchio, N.C., 2002. An overview of synchrotron radiation applications to low temperature geochemistry and environmental science. Rev. Mineral. Geochemistry 49, 1–69.
8. Carabante, I., Grahn, M., Holmgren, A., Hedlund, J., 2010. In situ ATR-FTIR studies on the competitive adsorption of arsenate and phosphate on ferrihydrite. J. Colloid Interface Sci. 351, 523–531.
9. Catalano, J.G., Park, C., Fenter, P., Zhang, Z., 2008. Simultaneous inner- and outer-sphere arsenate adsorption on corundum and hematite. Geochim. Cosmochim. Acta 72, 1986–2004.
10. Collins, C.R., Ragnarsdottir, K.V., Sherman, D.M., 1999. Effect of inorganic and organic ligands on the mechanism of cadmium sorption to goethite. Geochim. Cosmochim. Acta 63, 2989–3002.
11. Cornell, R.M., Schwertmann, U., 2003. The iron oxides: structure, properties, reactions, occurrences and uses. John Wiley Sons.
12. Das, S., Hendry, M. J., & Essilfie-Dughan, J., 2013. Adsorption of selenate onto ferrihydrite, goethite, and lepidocrocite under neutral pH conditions. Appl. Geochem. 28, 185–193.
13. Elzinga, E.J., Kretzschmar, R., 2013. In situ ATR-FTIR spectroscopic analysis of the co-adsorption of orthophosphate and Cd(II) onto hematite. Geochim. Cosmochim. Acta 117, 53–64.
14. Elzinga, E.J., Sparks, D.L., 2007. Phosphate adsorption onto hematite: An in situ ATR-FTIR investigation of the effects of pH and loading level on the mode of phosphate surface complexation. J. Colloid Interface Sci. 308, 53–70.
15. Farley, K.J., Dzombak, D.A., Morel, F.M., 1985. A surface precipitation model for the sorption of cations on metal oxides. J. Colloid Interface Sci. 106, 226–242.
16. Foerstendorf, H., Jordan, N., Heim, K., 2014. Probing the surface speciation of uranium (VI) on iron (hydr)oxides by in situ ATR FTIR spectroscopy. J. Colloid Interface Sci. 416, 133–138.
17. Hiemstra, T., 2018. Ferrihydrite interaction with silicate and competing oxyanions:

Geometry and Hydrogen bonding of surface species. Geochim. Cosmochim. Acta 238, 453–476.
18. Hiemstra, T., Riemsdijk, W.H. Van, Rossberg, A., Ulrich, K.U., 2009. A surface structural model for ferrihydrite II: Adsorption of uranyl and carbonate. Geochim. Cosmochim. Acta 73, 4437–4451.
19. Hiemstra, T., Van Riemsdijk, W.H., 2009. A surface structural model for ferrihydrite I: Sites related to primary charge, molar mass, and mass density. Geochim. Cosmochim. Acta 73, 4423–4436.
20. Hinkle, M.A., Wang, Z., Giammar, D.E., Catalano, J.G., 2015. Interaction of Fe(II) with phosphate and sulfate on iron oxide surfaces. Geochim. Cosmochim. Acta 158, 130–146.
21. Jambor, J.L., Dutrizac, J.E., 1998. Occurrence and constitution of natural and synthetic ferrihydrite, a widespread iron oxyhydroxide. Chem. Rev. 98, 2549–2586.
22. Jiang, W., Lv, J., Luo, L., Yang, K., Lin, Y., Hu, F., Zhang, J., Zhang, S., 2013. Arsenate and cadmium co-adsorption and co-precipitation on goethite. J. Hazard. Mater. 262, 55–63.
23. Jiang, Z., Liu, Q., Roberts, A.P., Barrón, V., Torrent, J., Zhang, Q., 2018. A new model for transformation of ferrihydrite to hematite in soils and sediments. Geology 46, 987–990.
24. Kim, J., Li, W., Philips, B.L., Grey, C.P., 2011. Phosphate adsorption on the iron oxyhydroxides goethite (α-FeOOH), akaganeite (β-FeOOH), and lepidocrocite (γ-FeOOH): a ^{31}P NMR Study. Energy Environ. Sci. 4, 4298–4305.
25. Komárek, M., Antelo, J., Králová, M., Veselská, V., Číhalová, S., Chrastný, V., Ettler, V., Filip, J., Yu, Q., Fein, J.B., Koretsky, C.M., 2018. Revisiting models of Cd, Cu, Pb and Zn adsorption onto Fe(III) oxides. Chem. Geol. 493, 189–198.
26. Kubicki, J.D., Paul, K.W., Kabalan, L., Zhu, Q., Mrozik, M.K., Aryanpour, M., Pierre-Louis, A.M., Strongin, D.R., 2012. ATR-FTIR and density functional theory study of the structures, energetics, and vibrational spectra of phosphate adsorbed onto goethite. Langmuir 28, 14573–14587.
27. Lee, J.C., Kim, E.J., Kim, H.W., Baek, K., 2016. Oxalate-based remediation of arsenic bound to amorphous Fe and Al hydrous oxides in soil. Geoderma 270, 76–82.
28. Ler, A., Stanforth, R., 2003. Evidence for surface precipitation of phosphate on goethite. Environ. Sci. Technol. 37, 2694–2700.
29. Li, L., Stanforth, R., 2000. Distinguishing adsorption and surface precipitation of phosphate on goethite (α-FeOOH). J. Colloid Interface Sci. 230, 12–21.
30. Li, W., Zhang, S., Shan, X.Q., 2007. Surface modification of goethite by phosphate for enhancement of Cu and Cd adsorption. Colloids Surfaces A Physicochem. Eng. Asp. 293, 13–19.
31. Lin, J., Zhan, Y., Wang, H., Chu, M., Wang, C., He, Y., Wang, X., 2017. Effect of calcium ion on phosphate adsorption onto hydrous zirconium oxide. Chem. Eng. J. 309, 118–129.
32. Liu, J., Zhu, R., Liang, X., Ma, L., Lin, X., Zhu, J., He, H., Parker, S.C., Molinari, M., 2018. Synergistic adsorption of Cd(II) with sulfate/phosphate on ferrihydrite: An in situ ATR-FTIR/2D-COS study. Chem. Geol. 477, 12–21.
33. Liu, J., Zhu, R., Xu, T., Xu, Y., Ge, F., Xi, Y., Zhu, J., He, H., 2016. Co-adsorption of phosphate and zinc(II) on the surface of ferrihydrite. Chemosphere 144, 1148–1155.
34. Luengo, C., Brigante, M., Antelo, J., Avena, M., 2006. Kinetics of phosphate adsorption on goethite: Comparing batch adsorption and ATR-IR measurements. J. Colloid Interface Sci. 300, 511–518.

694 35. Michel, F.M., Ehm, L., Antao, S.M., Lee, P.L., Chupas, P.J., Liu, G., Strongin, D.R.,
695 Schoonen, M.A.A., Phillips, B.L., Parise, J.B., 2007. The Structure of ferrihydrite, a
696 nanocrystalline material. Science. 316, 1726 LP – 1729.
697 36. Milton, C., Murata, K.J., Knechtel, M.M., 1944. Weinschenkite, yttrium phosphate
698 dihydrate, from virginia. Am. Mineral. 29, 92–107.
699 37. Murphy, J., Riley, J.P., 1962. A modified single solution method for the determination of
700 phosphate in natural waters. Anal. Chim. Acta 27, 31–36.
701 38. Navrotsky, A., Mazeina, L., Majzlan, J., 2008. Size-driven structural and thermodynamic
702 complexity in iron oxides. Science 319, 1635–1638.
703 39. Noda, I., 2014. Frontiers of two-dimensional correlation spectroscopy. Part 1. New
704 concepts and noteworthy developments. J. Mol. Struct. 1069, 3–22.
705 40. Nooney, M.G., Campbell, A., Murrell, T.S., Lin, X., Hossner, L.R., Chusuei, C.C.,
706 Goodman, D.W., 1998. Nucleation and growth of phosphate on metal oxide thin films.
707 Langmuir 14, 2750–2755.
708 41. Ona-Nguema, G., Morin, G., Juillot, F., Calas, G., Brown, G.E., 2005. EXAFS analysis of
709 arsenite adsorption onto two-line ferrihydrite, hematite, goethite, and lepidocrocite.
710 Environ. Sci. Technol. 39, 9147–9155.
711 42. Ostergren, J.D., Trainor, T.P., Bargar, J.R., Brown, G.E., Parks, G.A., 2000. Inorganic
712 ligand effects on Pb (II) sorption to goethite (α-FeOOH): I. Carbonate. J. Colloid Interface
713 Sci., 225(2), 466–482.
714 43. Pinney, N., Kubicki, J.D., Middlemiss, D.S., Grey, C.P., Morgan, D., 2009. Density
715 functional theory study of ferrihydrite and related Fe-oxyhydroxides. Chem. Mater. 21,
716 5727–5742.
717 44. Pivovarov, S., 2001. Adsorption of cadmium onto hematite: Temperature dependence. J.
718 Colloid Interface Sci. 234, 1–8.
719 45. Ponthieu, M., Juillot, F., Hiemstra, T., van Riemsdijk, W.H., Benedetti, M.F., 2006. Metal
720 ion binding to iron oxides. Geochim. Cosmochim. Acta 70, 2679–2698.
721 46. Rietra, R.P., Hiemstra, T., Van Riemsdijk, W.H., 2001. Interaction between calcium and
722 phosphate adsorption on goethite. Env. Sci.Technol. 35, 3369–3374.
723 47. Rout, K., Mohapatra, M., Anand, S., 2012. 2-Line ferrihydrite: Synthesis, characterization
724 and its adsorption behaviour for removal of Pb(ii), Cd(ii), Cu(ii) and Zn(ii) from aqueous
725 solutions. Dalt. Trans. 41, 3302–3312.
726 48. Santoro, V., Martin, M., Persson, P., Lerda, C., Said-Pullicino, D., Magnacca, G., Celi, L.,
727 2019. Inorganic and organic P retention by coprecipitation during ferrous iron oxidation.
728 Geoderma 348, 168–180.
729 49. Silva-Yumi, J., Escudey, M., Gacitua, M., Pizarro, C., 2018. Kinetics, adsorption and
730 desorption of Cd(II) and Cu(II) on natural allophane: Effect of iron oxide coating.
731 Geoderma 319, 70–79.
732 50. Simanova, A.A., Loring, J.S., Persson, P., 2011. Formation of ternary metal-oxalate surface
733 complexes on α-FeOOH particles. J. Phys. Chem. C 115, 21191–21198.
734 51. Singh, A., Catalano, J.G., Ulrich, K.U., Giammar, D.E., 2012. Molecular-scale structure of
735 uranium(VI) immobilized with goethite and phosphate. Environ. Sci. Technol. 46, 6594–
736 6603.
737 52. Swedlund, P.J., Webster, J.G., Miskelly, G.M., 2009. Goethite adsorption of Cu(II), Pb(II),
738 Cd(II), and Zn(II) in the presence of sulfate: Properties of the ternary complex. Geochim.
739 Cosmochim. Acta 73, 1548–1562.

53. Tejedor-tejedor, M.I., Anderson, M.A., 1990. The protonation of phosphate on the surface of goethite as studied by CIR-FTIR and electrophoretic mobility. Langmuir 6, 602–611.
54. Tiberg, C., Gustafsson, J.P., 2016. Phosphate effects on cadmium(II) sorption to ferrihydrite. J. Colloid Interface Sci. 471, 103–111.
55. Tiberg, C., Sjöstedt, C., Persson, I., & Gustafsson, J. P. (2013). Phosphate effects on copper (II) and lead (II) sorption to ferrihydrite. Geochim. Cosmochim. Acta, 120, 140–157.
56. Trivedi, P. and Axe, L. 2001. Predicting divalent metal sorption to hydrous Al, Fe, and Mn oxides. Environ. Sci. Technol. 35, 1779–1784.
57. Villalobos, M., Trotz, M. a, Leckie, J.O., 2001. Surface complexation modeling of carbonate effects on the adsorption of Cr (VI), Pb (II), and U (VI) on goethite. Environ. Sci. Technol. 35, 3849–3856.
58. Wade, J., Waterhouse, H., Roche, L.M., Horwath, W.R., 2018. Structural equation modeling reveals iron (hydr)oxides as a strong mediator of N mineralization in California agricultural soils. Geoderma 315, 120–129.
59. Wang, C., Cui, Y., Zhang, J., Gomez, M., Wang, S., Jia, Y., 2018. Occurrence state of co-existing arsenate and nickel ions at the ferrihydrite-water interface: Mechanisms of surface complexation and surface precipitation via ATR-IR spectroscopy. Chemosphere 206, 33–42.
60. Wang, H., Zhu, J., Fu, Q., Hu, H., 2015. Adsorption of phosphate on pure and humic acid-coated ferrihydrite. J. Soils Sediments 1500–1509.
61. Wang, K., Xing, B., 2004. Mutual effects of cadmium and phosphate on their adsorption and desorption by goethite. Environ. Pollut. 127, 13–20.
62. Wang, X., Liu, F., Tan, W., Li, W., Feng, X., Sparks, D.L., 2013. Characteristics of phosphate adsorption-desorption onto ferrihydrite : comparison with well-crystalline Fe (hydr)oxides. Soil Sci. 178, 1–11.
63. Xu, T., Zhu, R., Shang, H., Xia, Y., Liu, X., Zhang, L., 2019. Photochemical behavior of ferrihydrite-oxalate system: Interfacial reaction mechanism and charge transfer process. Water Res. 159, 10–19.
64. Yan, L., Zhu, R., Liu, J., Yang, Y., Zhu, J., Sun, H.J., He, H., 2020. Effects of fullerol and graphene oxide on the phase transformation of two-line ferrihydrite. ACS Earth Sp. Chem.
65. Yang, Y., Wang, S., Xu, Y., Zheng, B., Liu, J., 2016. Molecular-scale study of aspartate adsorption on goethite and competition with phosphate. Environ. Sci. Technol. 50, 2938–2945.
66. Zhang, T., Zeng, X., Zhang, H., Lin, Q., Su, S., Wang, Y., Bai, L., Wu, C., 2019. The effect of the ferrihydrite dissolution/transformation process on mobility of arsenic in soils: Investigated by coupling a two-step sequential extraction with the diffusive gradient in the thin films (DGT) technique. Geoderma 352, 22–32.
67. Zhu, Y., Zhu, R., Yan, L., Fu, H., Xi, Y., Zhou, H., Zhu, G., Zhu, J., He, H., 2018. Visible-light Ag/AgBr/ferrihydrite catalyst with enhanced heterogeneous photo-Fenton reactivity via electron transfer from Ag/AgBr to ferrihydrite. Appl. Catal. B Environ. 239, 280–289.